ADVANCED ENERGY MATERIALS
www.advenergymat.de

Platinum/Tantalum Carbide Core–Shell Nanoparticles with Sub-Monolayer Shells for Methanol and Oxygen Electrocatalysis

Zhenshu Wang, Jin Soo Kang, Daniel Göhl, Paul Paciok, Danelle S. Gonçalves, Hyung-Kyu Lim, Daniela Zanchet, Marc Heggen, Yang Shao-Horn,* Marc Ledendecker,* and Yuriy Román-Leshkov**

Core–shell architectures provide great opportunities to improve catalytic activity, but achieving nanoparticle stability under electrochemical cycling remains challenging. Herein, core–shell nanoparticles comprising atomically thin Pt shells over earth-abundant TaC cores are synthesized and used as highly durable electrocatalysts for the methanol oxidation reaction (MOR) and the oxygen reduction reaction (ORR) needed to drive direct methanol fuel cells (DMFCs). Characterization data show that a thin oxidic passivation layer protects the TaC core from undergoing dissolution in the fuel cell-relevant potential range, enabling the use of partially covered Pt/TaC core–shell nanoparticles for MOR and ORR with high stability and enhanced catalytic performance. Specifically, at the anode the surface-oxidized TaC further enhances MOR activity compared to conventional Pt nanoparticles. At the cathode, the Pt/TaC catalyst feature increases tolerance to methanol crossover. These results show unique synergistic advantages of the core–shell particles and open opportunities to tailor catalytic properties for electrocatalytic reactions.

1. Introduction

Direct methanol fuel cells (DMFCs), involving the methanol oxidation reaction (MOR) at the anode and the oxygen reduction reaction (ORR) at the cathode, offer unique advantages, particularly for small devices, over hydrogen fuel cells due to methanol's high volumetric energy density and ease of storage.[1–3] However, despite using state-of-the-art precious metal catalysts in both electrodes, the kinetics of MOR and ORR are sluggish and limit the overall cell performance.[2,4–6] Therefore, enhancing activity, and stability, while minimizing the use of critical materials is necessary for the large-scale implementation of DMFCs. Pt/transition metal

Z. Wang, J. S. Kang, Y. Román-Leshkov
Department of Chemical Engineering
Massachusetts Institute of Technology
Cambridge, MA 02139, USA
E-mail: jinsookang@snu.ac.kr; yroman@mit.edu

J. S. Kang, Y. Shao-Horn
Research Laboratory of Electronics
Massachusetts Institute of Technology
Cambridge, MA 02139, USA
E-mail: shaohorn@mit.edu

J. S. Kang
Department of Energy Systems Engineering
Department of Energy Resources Engineering & Research Institute of Energy and Resources
Seoul National University
Seoul 08826, Republic of Korea

The ORCID identification number(s) for the author(s) of this article can be found under https://doi.org/10.1002/aenm.202304092

DOI: 10.1002/aenm.202304092

D. Göhl, M. Ledendecker
Department of Chemistry
Ernst-Berl-Institut für Technische und Makromolekulare Chemie
Technical University of Darmstadt
64287 Darmstadt, Germany
E-mail: marc.ledendecker@tum.de

P. Paciok, M. Heggen
Ernst Ruska-Center for Microscopy and Spectroscopy with Electrons and Peter Grünberg Institute
Forschungszentrum Jülich GmbH
52425 Jülich, Germany

D. S. Gonçalves, D. Zanchet
Institute of Chemistry
University of Campinas
SP 13083-970, Brazil

H.-K. Lim
Division of Chemical Engineering and Bioengineering
Kangwon National University
Chuncheon, Gangwon-do 24341, Republic of Korea

Y. Shao-Horn
Department of Mechanical Engineering & Department of Materials Science and Engineering
Massachusetts Institute of Technology
Cambridge, MA 02139, USA

carbide (TMC) core–shell nanoparticles pioneered by Román–Leshkov and co-workers show promise in this respect.[7] For example, the Ti-doped WC (TiWC) core covered with Pt or PtRu shell showed superior performance in ORR and MOR, respectively, when compared to benchmark Pt-based catalysts.[7,8] However, the TiWC core undergoes dissolution when it is in direct contact with acidic electrolytes under ORR conditions, which is hardly avoidable during DMFC operation.[8]

The chemical stability of various TMCs has been comprehensively studied by Chen and co-workers, who demonstrated that the durability of TMCs is correlated with the stability of the oxide passivation layer on the surface that forms spontaneously over these materials under oxidizing potentials.[9,10] In general, TMCs with parent metals that bind strongly to oxygen are more stable under electrochemical cycling. Recently, Göhl, Ledendecker, and co-workers demonstrated that the transition metal-carbon bond enthalpies govern the electrochemical stability of TMCs, finding that titanium, tantalum, and zirconium carbides have high stability in acid,[11,12] which is in line with previous observations.[9,10] On the other hand, because thermal carburization of oxide-based precursors is an essential step for the synthesis of TMC-based nanoparticles, a strong interaction between the transition metal and oxygen is unfavorable in terms of synthetic feasibility because of the increasingly higher temperatures required for carburization. Among the TMCs that are stable in acid, tantalum carbide has a relatively low oxygen binding energy.[10] Thus, we surmised that tantalum carbide is a suitable core material for Pt/TMC core shells, satisfying both synthetic viability and stability in acidic environments. Meanwhile, synthesis of tantalum carbide nanoparticles often requires a temperature above 1200 °C,[13,14] and to the best of our knowledge, tantalum carbide interfaced with Pt has not been synthesized directly owing to the low Tammann temperature of Pt, which would promote significant sintering at the temperature needed for TaC synthesis.

In this study, Pt/TaC core–shell nanoparticles were synthesized and were applied as highly active and stable electrocatalysts for both MOR and ORR, targeting their potential applications in DMFCs. The synthesis used a high-temperature self-assembly method pioneered by our group,[7] which enabled Pt monolayers (MLs) to form over the nanosized TaC particles during thermal carburization and mitigated the needed synthesis temperature down to below 1000 °C. Pt/TaC catalysts with sub-ML shell coverages had superior activity in MOR compared to that of bare Pt. In addition, Pt/TaC nanoparticles showed significantly enhanced ORR performance in the presence of methanol, which is necessary due to methanol crossover under realistic DMFC operating conditions. Lastly, the high stability of Pt/TaC under electrochemical operation conditions was investigated using various analytical techniques.

M. Ledendecker
Department of Sustainable Energy Materials
Technical University of Munich, Campus Straubing for Biotechnology and Sustainability
94315 Straubing, Germany

2. Results and Discussion

2.1. Synthesis and Characterization of Pt/TaC Nanoparticles

The synthesis route of Pt/TaC core–shell nanoparticles via a high-temperature self-assembly method is summarized as a scheme in **Figure 1**. First, TaO_x nanoparticles were prepared in a reverse microemulsion by hydrolysis of tantalum isopropoxide. The Pt precursor was added in a separate, smaller reverse microemulsion batch serving as the shell component. Then, the particles were encapsulated by a silica shell and subjected to thermal carburization at 970 °C in a tube furnace under the flow of a gas mixture of 80% H_2 and 20% CH_4, to reduce and carburize TaO_x. Prior work had reported TaO_x carburization temperatures above 1200 °C;[13,14] however, we hypothesize that Pt facilitates the TaO_x reduction via H_2 spillover and decomposition of CH_4, which serves as the carbon source, thereby substantially decreasing the carburization temperature.[15–18] Pt/TaC nanoparticles supported on carbon were subsequently obtained by dissolving the silica shell using ethanol-diluted hydrofluoric acid solution and then dispersing the particles onto a carbon black support. Pt/TaC nanoparticles with four different shell thicknesses were prepared by using different amounts of Pt precursors. As a reference catalyst, we used commercial carbon-supported Pt nanoparticles (20 wt%, Premetek), which are hereafter denoted as Pt_{comm}.

From the powder X-ray diffraction (PXRD) patterns displayed in **Figure 2a**, signals from phase-pure TaC (PDF no. 00-035-0801) were clearly observed from Pt/TaC nanoparticles while reflections from Pt were not apparent. The PXRD analysis of bare TaC nanoparticles (synthesized at 100 °C higher temperature compared to Pt/TaC) was also carried out (Figure S1, Supporting Information), and the result matched well with the TaC peaks of Pt/TaC. From the crystallite sizes calculated from PXRD patterns and the Pt:Ta ratio obtained from inductively coupled plasma-mass spectroscopy (ICP-MS), Pt shell thicknesses of the nanoparticles were estimated as 0.2, 0.6, 0.9, and 1.2 ML (see Table S1, Supporting Information, for details), and the Pt/TaC nanoparticles were named Pt/TaC_0.2 ML, Pt/TaC_0.6 ML, Pt/TaC_0.9 ML, and Pt/TaC_1.2 ML, respectively. The uniformity of the synthesized particles was imperfect; the morphologies of Pt/TaC were characterized by transmission electron microscopy (TEM) analysis, which clearly showed carbon-supported nanoparticles ranging in size from 5 to 20 nm (Figure 2b; Figure S2, Supporting Information). However, the nanoparticles were expected to manifest different electrocatalytic behaviors on average with regard to the calculated Pt ML coverage. The wetting of Pt on the TaC surface was confirmed by aberration-corrected scanning transmission electron microscopy (STEM) and the corresponding elemental maps acquired by energy-dispersive X-ray spectroscopy (EDX) displayed in Figure 2c,d (and by additional images shown in Figures S3 and S4, Supporting Information; Figure 5a in the later section), respectively.

In order to obtain insights into the chemical state of Pt and TaC with varying shell thicknesses, diverse X-ray techniques were employed. Figure 2e shows the X-ray absorption near-edge structure (XANES) spectra of Pt_{comm} and Pt/TaC nanoparticles obtained at the Pt L_2-edge. Although XANES at the Pt L_3-edge is mostly measured as it gives a large amount of information on

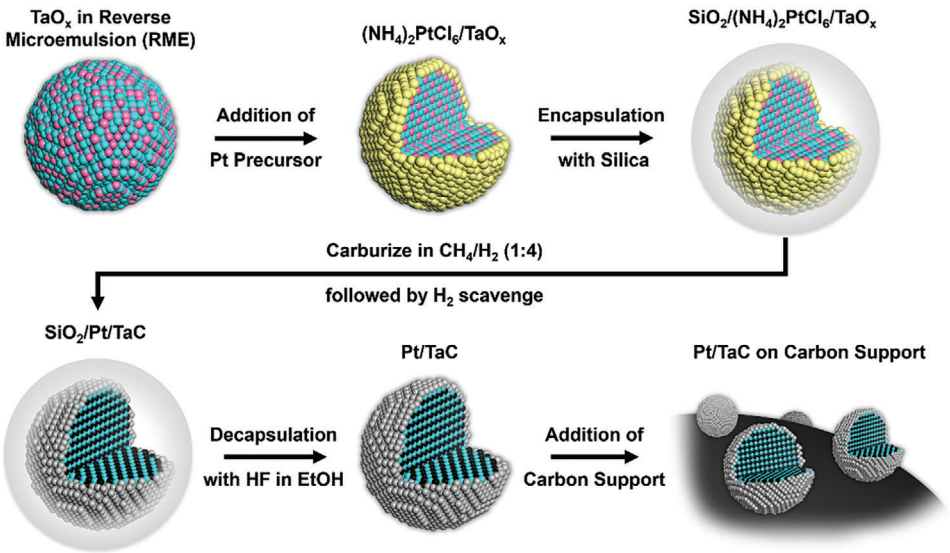

Figure 1. Synthesis of Pt/TaC core–shell nanoparticles. Schematic overview of the synthetic procedure based on the self-assembly of Pt on TaC during thermal carburization. Silica encapsulation was carried out prior to the carburization to inhibit nanoparticle sintering at high temperatures, and the silica shell was removed before the incorporation of carbon supports. Color codes: cyan Ta, magenta O, yellow $(NH_4)_2PtCl_6$, gray Pt, black C.

the 5d states, the L_2-edge was selected because the Ta L_1- and L_2-edges are located close to the Pt L_3-edge and are entangled in the measurement. Nonetheless, prior literature reports indicate that XANES data obtained at the Pt L_2 edge represent the electronic structures reasonably well.[19–22] Note the white line intensity was significantly larger for Pt/TaC as compared to that of Pt_{comm} and increases further with decreasing shell thicknesses. This observation was in line with the trend in the Pt 4f spectra acquired by X-ray photoelectron spectroscopy (XPS) analysis, which showed a larger positive shift for smaller shell thicknesses (Figure S5, Supporting Information). Based on the work functions of Pt and TaC,[23–25] it is unlikely that Pt would lose charge to TaC and, previously, we thoroughly discussed the genesis of the Pt d-band broadening and the corresponding increase in the white line intensity when the coupling matrix element of TMC's parent metal is larger than that of Pt.[22] According to the work by Hammer and Nørskov, Ta has a larger coupling matrix element than Pt, and this leads to the broadening of the Pt d-band when the formation of a chemical bond between Pt and Ta takes place.[26,27] Therefore, we expect a downshift of the Pt d-band center with regard to the Fermi level, given that the d-band filling should be conserved. Density functional theory (DFT) calculations for the projected density of states of Pt d-band were performed at Pt (111) and Pt/TaC (100) surfaces (Figures S6 and S7, Supporting Information), whose d-band centers were estimated as −2.60 and −2.93 eV versus their Fermi energy levels, respectively.

The observed trend in Pt-surface coverage was indirectly corroborated by comparing the signals from the carbidic and oxidic features in the Ta 4f XPS spectra (Figure S8, Supporting Information). When the nominal Pt-shell thickness increases, the shell increases in homogeneity and a smaller amount of native oxide can be found. In order to investigate the geometric characteristics of the Pt shell on the TaC core, extended X-ray absorption fine structure (EXAFS) analysis was carried out (Figure 2f). It is known that an increase/decrease in the interatomic distance of Pt atoms results in the broadening/narrowing of Pt d-band and a consequent downshift/upshift of the d-band center.[27–29] By fitting the EXAFS spectra (detailed fitted parameters are displayed in Table S2, Supporting Information), we could compare Pt-Pt distances among Pt_{comm} and Pt/TaC nanoparticles. Although the lattice parameter of face-centered cubic (fcc) Pt (0.39 nm) is smaller than that of TaC (0.44 nm), the presence of the TaC core did not induce notable changes to the Pt-Pt distance. This result indicates that the modifications of the Pt d-band structure observed by both XANES and XPS are mostly attributable to the electronic interaction between Pt and TaC.

2.2. Methanol Oxidation Characteristics of Pt/TaC Nanoparticles

Considering the potential application of Pt/TaC at the anode for DMFCs, catalyst performance in MOR was first characterized by cyclic voltammetry (CV) measurements in 0.1 M $HClO_4$ containing 1.0 M methanol (insets of **Figure 3**a,b). We compared current densities at 0.5, 0.6, and 0.7 V versus reversible hydrogen electrode (RHE; all of the electrochemical potentials are hereafter noted with regard to RHE unless otherwise stated) to obtain specific and mass activities, because background corrections were not viable in the potential range below 0.45 V (Figure S9, Supporting Information).[30–32] Figure 3a,b compares specific and mass activities of Pt_{comm} and Pt/TaC nanoparticles in MOR. Pt/TaC with relatively thin (0.2 and 0.6 ML) shells manifested higher MOR activities (both mass and specific) as compared to Pt_{comm}, while those with 0.9 and 1.2 ML-thick shells showed lower activity. At 0.5 V, Pt/TaC_0.2 ML was the most active catalyst, but Pt/TaC_0.6 ML had superior activity at higher potentials. Since potential interference from capacitive currents is expected to be larger when the overall current density is smaller (i.e., at lower potentials), we selected Pt/TaC_0.6 ML as the

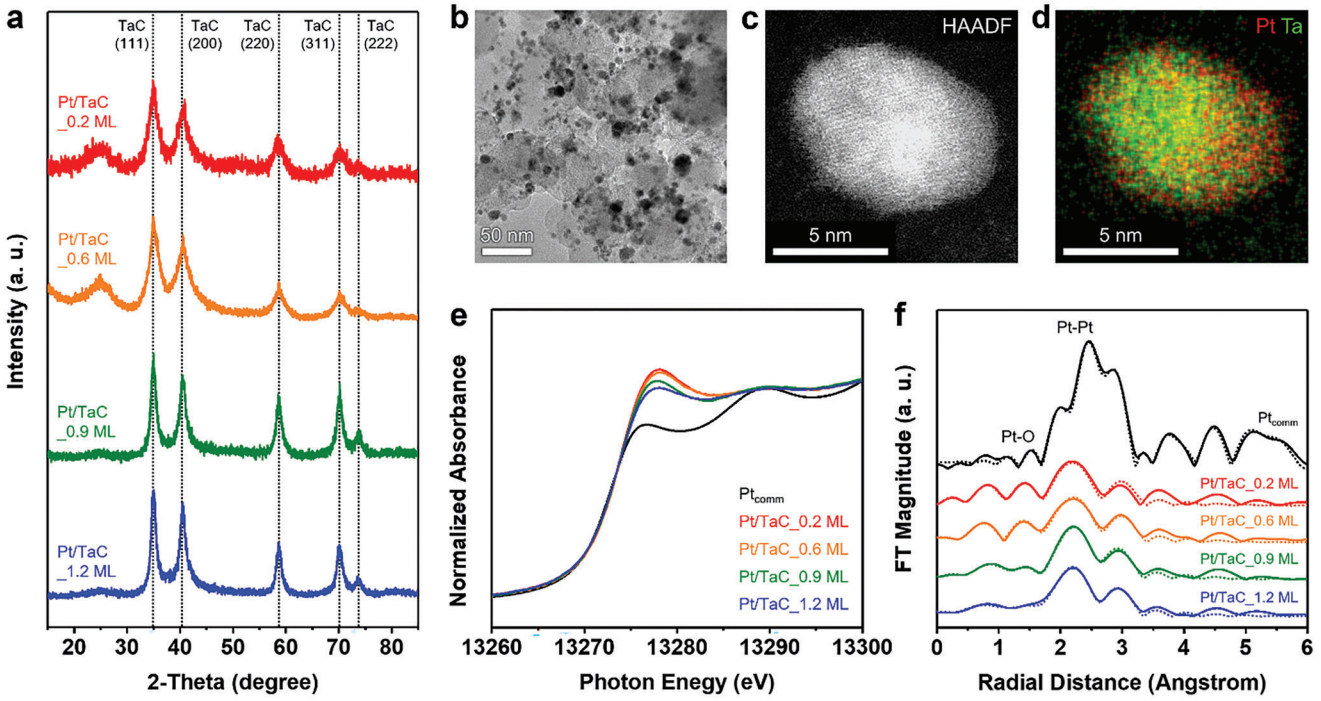

Figure 2. Materials characterization of Pt/TaC core–shell nanoparticles. a) PXRD patterns of Pt/TaC core–shell nanoparticles with various shell thicknesses. All patterns were collected from powder samples at a scan rate of 4 °C min^{-1}, and the patterns were indexed with regard to the crystal structure of TaC (PDF no. 00-035-0801). b) Low-magnification TEM image of Pt/TaC_0.6 ML. c) High-magnification STEM image of Pt/TaC_0.6 ML obtained by using a high-angle annular dark-field (HAADF) detector and d) corresponding elemental EDX map showing the distributions of Pt and Ta. e) XANES and f) Fourier transform of EXAFS spectra of Pt$_{comm}$ and Pt/TaC nanoparticles acquired at the Pt L_2-edge in transmittance mode; solid and dotted lines in the panel (e) show experimental data and the fitted results, respectively.

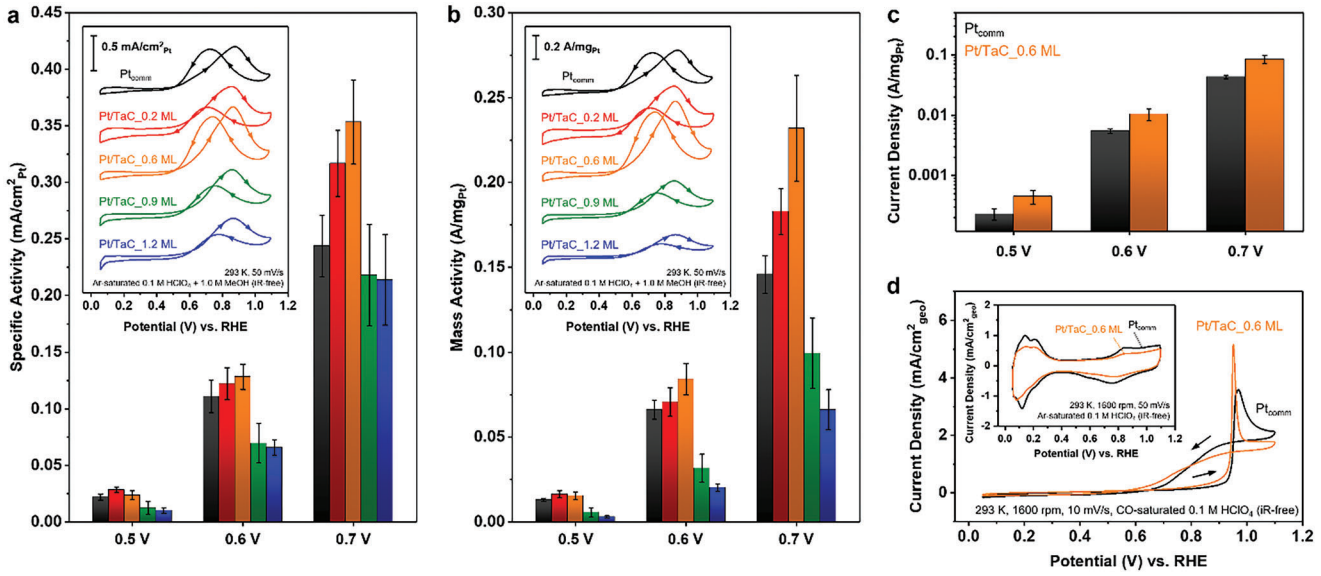

Figure 3. Electrochemical methanol and CO oxidation characteristics. a) Specific and b) mass MOR activities of Pt$_{comm}$ and Pt/TaC core–shell nanoparticles obtained by MOR CV diagrams displayed in the insets; the CV measurements were carried out in Ar-saturated 0.1 M $HClO_4$ containing 1.0 M MeOH at a scan rate of 50 mV s^{-1} without convection. Calculations of activities were performed after the subtraction of background currents. c) Summary of mass MOR activities of Pt$_{comm}$ and Pt/TaC_0.6 ML from steady-state measurements at various potentials (data shown in Figure S11, Supporting Information). d) CO bulk oxidation characteristics of Pt$_{comm}$ and Pt/TaC_0.6 ML in CO-saturated 0.1 M $HClO_4$ measured at a scan rate of 10 mV s^{-1} and a rotation speed of 1600 rpm; the inset shows CV diagrams obtained without the presence of CO. Error bars show standard deviations obtained from at least three independent measurements.

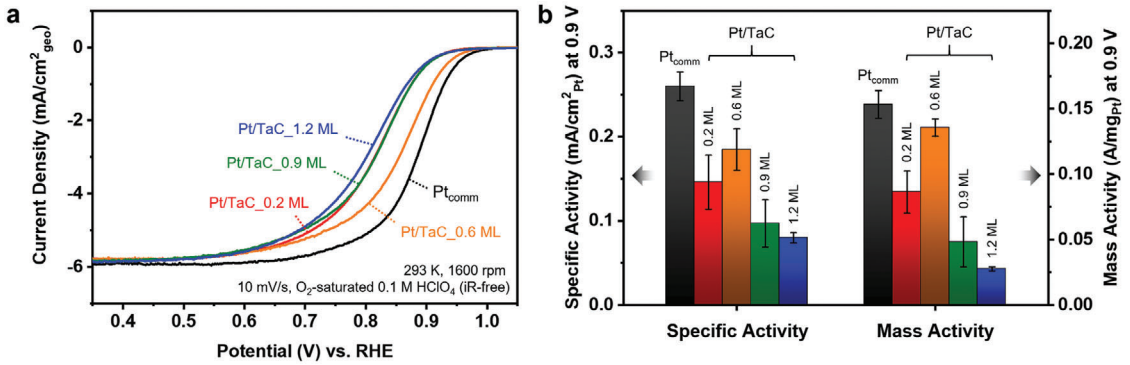

Figure 4. Electrochemical oxygen reduction characteristics. a) ORR polarization curves of Pt_{comm} and Pt/TaC core–shell nanoparticles with various shell thicknesses. All of the measurements were carried out in O_2-saturated 0.1 M $HClO_4$ at a scan rate of 10 mV s^{-1} and a rotation speed of 1600 rpm. The polarization curves were obtained by subtraction of capacitive currents. b) Specific and mass ORR activities of Pt_{comm} and Pt/TaC core–shell nanoparticles at 0.9 V. Error bars show standard deviations obtained from at least three independent measurements.

best-performing catalysts and used it for further investigations. Pt/TaC had lower MOR activities compared to those of commercial carbon-supported PtRu nanoparticles (alloyed in 1:1 atomic ratio, 20 wt%, Premetek; hereafter denoted as $PtRu_{comm}$), though the mass activities were comparable when Ru was included in the mass-normalization (Figure S10, Supporting Information).

We carried out chronoamperometry measurements of Pt_{comm} and Pt/TaC_0.6 ML catalysts at 0.5, 0.6, and 0.7 V (Figure S11a,b, Supporting Information). Specific and mass activities were calculated using the current density at 10 min, and they are displayed in Figure S11c (Supporting Information) and Figure 3c, respectively. At steady–state, Pt/TaC_0.6 ML clearly featured higher MOR activity compared to Pt_{comm}.

In light of these results, we then explored the origin of the high MOR activity of Pt/TaC catalysts. It is known that MOR mostly proceeds via methanol dehydrogenation followed by CO oxidation.[33] Kinetically, the CO oxidation step is rate-limiting on Pt surfaces.[34] Figure 3d shows CO bulk oxidation characteristics of Pt_{comm} and Pt/TaC_0.6 ML measured in a CO-saturated 0.1 M $HClO_4$ electrolyte. CO oxidation on Pt/TaC_0.6 ML took place at an earlier potential relative to that on Pt_{comm}, indicating that Pt/TaC has weaker CO binding. This is consistent with the Pt characterization results showing an increased white line intensity in XANES and a positive shift of Pt 4f spectra in XPS. CO oxidation on Pt takes place via a Langmuir-Hinshelwood mechanism where neighboring, adsorbed -OH groups react with adsorbed -CO to form CO_2.[35] The inset of Figure 3d shows the CV curves of Pt_{comm} and Pt/TaC_0.6 ML measured in Ar-saturated 0.1 M $HClO_4$, from which an insignificant difference in -OH formation on Pt_{comm} and Pt/TaC could be observed. From these results, a change in CO adsorption characteristics by the presence of TaC could be regarded as one of the reasons for superior MOR performance in Pt/TaC nanocatalysts, Indeed, electronic interactions between TaC core and Pt shell, which presumably leads to the downshift of Pt d-band center, can reduce CO adsorption strength on the Pt surface and enhance the overall CO oxidation performance. This was corroborated by the estimated CO adsorption energies on Pt (111) and Pt/TaC (100) surfaces (Figure S6, Supporting Information) from DFT calculations (Table S3, Supporting Information), though the difference was not

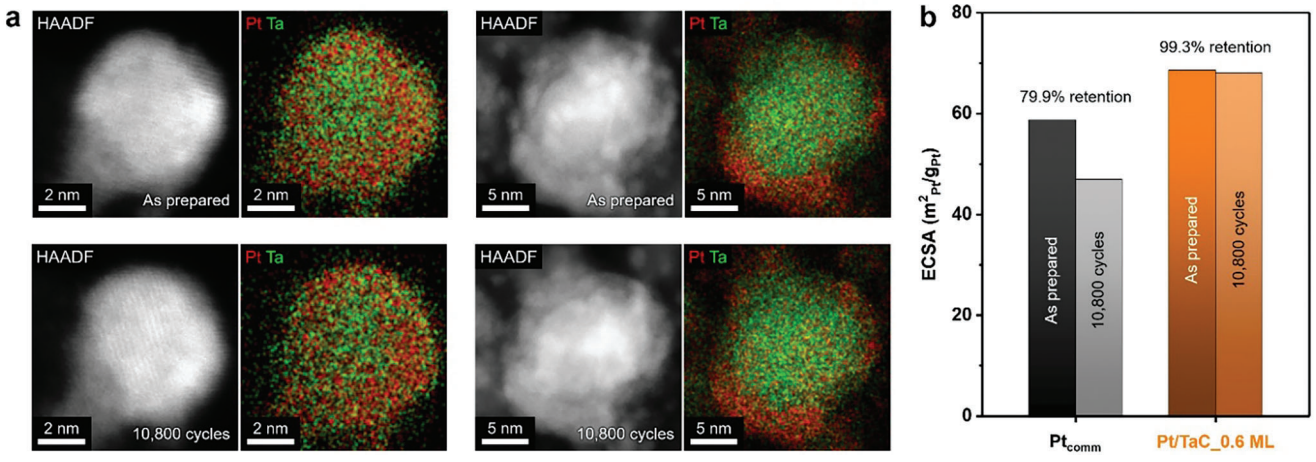

Figure 5. Structural stability of Pt/TaC core–shell nanoparticles. a) IL-STEM images and corresponding elemental EDX maps of Pt/TaC_0.6 ML before and after 10 800 AST cycles in Ar-saturated 0.1 M $HClO_4$ from 0.4 to 1.0 V with a scan rate of 1.0 V s^{-1}. b) ECSAs of Pt_{comm} and Pt/TaC_0.6 ML before and after the AST in O_2-saturated 0.1 M $HClO_4$ electrolyte at the same potential range and the scan rate. ECSAs were calculated from the H_{upd} region in Figure S20 (Supporting Information).

substantial. We additionally obtained CO stripping results of Pt_{comm} and Pt/TaC_0.6 ML and verified that Pt/TaC is more resistant to CO poisoning (Figure S12, Supporting Information).

In addition to the weaker CO binding, the specific MOR activities of Pt/TaC with nearly complete Pt-coverage (0.9 and 1.2 ML) were similar, but both were lower than that of Pt_{comm} (Figure 3a). Given that the Pt shell exhibited similar electronic structure changes as those found for subML coverages (Figure 2e), it appears that electronic interactions between TaC and Pt alone cannot explain the enhanced MOR performance for Pt/TaC_0.6 ML. We hypothesize the TaC surface exposed to the electrolyte plays a critical role in enhancing MOR activity. In the MOR potential region, an oxide passivation layer forms spontaneously on the surface of TaC,[10] enriching the surface with —OH groups. For shell thicknesses below 1 ML, CO oxidation can be facilitated by a bifunctional effect[32,36] at the interface between Pt and surface-exposed TaC, where the reaction between —CO on Pt and —OH on passivated TaC may take place (Figure S13a, Supporting Information). This surface composition matches well with the narrow CO bulk oxidation peak of Pt/TaC_0.6 relative to that of Pt_{comm}. The CO oxidation potential is dependent on facets and coordination environment in Pt_{comm},[37,38] and interfacial sites between Pt and TaC would provide a relatively uniform environment for CO oxidation. We carried out DFT calculations of OH adsorption energies on Pt (111), TaC (100), and Pt/TaC (100) surfaces, which unveiled that the formation of the —OH group is more favorable on the TaC compared to the Pt surfaces. This is in line with our hypothesis on the bifunctional enhancement of MOR for Pt/TaC with Pt shell coverage being less than 1 ML.

Meanwhile, when the shell coverage of Pt/TaC is close to or slightly larger than 1 ML, the influence of adsorbed —OH on the exposed TaC surface is not significant anymore. However, oxidation of TaC might occur to some extent through pinholes in the Pt shell, which is analogous to our previous observations from Pt/TiWC[22] and XPS results showing the presence of native TaO_x even when the thickness of the Pt shell is 1.2 ML (Figure S8, Supporting Information). The oxide layer that forms between TaC and Pt seems to be decreasing the overall electrical conductivity of the catalysts, leading to lower electrocatalytic activity for the Pt/TaC_0.9 ML and Pt/TaC_1.2 ML catalysts (Figure S13b, Supporting Information). Indeed, this hypothetical interpretation of our experimental observations regarding the origin of the MOR activity trend of the core–shell nanoparticles depending on the Pt shell coverage is currently the subject of active investigations in our groups.

2.3. Oxygen Reduction Characteristics and Electrochemical Stability of Pt/TaC

We evaluated Pt/TaC nanoparticles as catalysts for the cathodic ORR. **Figure 4a** shows the ORR polarization curves of Pt_{comm} and Pt/TaC with different shell thicknesses. Specific and mass activities were calculated at 0.9 V using the Koutecky–Levich equation,[39] and the results are summarized in Figure 4b. Pt/TaC nanoparticles were not as active as Pt_{comm} for the ORR, even when normalizing the current densities by the mass of Pt. In general, the adsorption of reaction intermediates in ORR is known to be stronger than the optimum at the surface of Pt catalysts.[40] For this reason, a Pt-based catalyst with a slightly weaker adsorption characteristic of the ORR intermediates, or with a small downshift in the d-band center position, was pursued to obtain a high catalytic activity.[41] Meanwhile, the experimental and theoretical results in this study imply that Pt/TaC has a downshifted d-band center, which does not match the inferior ORR performance. Interestingly, the binding of OH on Pt/TaC (100) was estimated to be stronger than that of OH on the Pt (111) surface from the DFT calculations (Table S3, Supporting Information). This indicates that reorganization of orbitals at local Pt clusters in the shell might have a larger influence on the catalytic activity of Pt/TaC, rather than their average electronic structures.

Based on the comparison among the Pt/TaC catalysts, the optimum Pt shell thickness was 0.6 ML in terms of the ORR performance, and Pt/TaC_0.6 ML was thereby selected for further studies. To gain insights into the role of the TaC in the reaction kinetics, ORR polarization curves were obtained under various rotation rates (Figure S14, Supporting Information), and electron transfer numbers of Pt_{comm} and the best-performing Pt/TaC core–shell nanoparticles (Pt/TaC_0.6 ML) were calculated by a Koutecky–Levich analysis (details are provided in the Supporting Information).[39,42,43] We obtained identical electron transfer numbers (4.08 electrons) for both Pt_{comm} and Pt/TaC_0.6 ML (Figure S15, Supporting Information) indicating that the reaction mechanism does not change in the presence of TaC. Similar Tafel slopes were also observed from the ORR characteristics of all catalysts investigated in this study (Figure S16, Supporting Information), though the Tafel slopes of Pt/TaC core–shell nanoparticles were larger than that of Pt_{comm} and the slope increased with thicker Pt shells.

Next, we explored the stability of Pt/TaC at conditions relevant to DMFC operation. Since the stability of fuel cell catalysts is mostly challenged by oxidative degradation at high potentials, we carried out various analyses under ORR conditions. First, Pt/TaC_0.6 ML was characterized before and after the accelerated stress test (AST; 10 800 potential cycles in 0.1 M $HClO_4$ within the potential range of 0.4 to 1.0 V at a scan rate of 1.0 V s^{-1}) by using identical location (IL)-STEM with corresponding elemental EDX mappings (**Figure 5a**; Figure S17, Supporting Information). The changes in morphology were negligible even after 10 800 potential cycles, and the elemental EDX maps clearly show that the locations of Pt and Ta did not change during the AST.

Moreover, the excellent stability of the TaC core was corroborated by comparing Pt/TaC_0.6 ML and Pt/TiWC reported in our previous studies[7,8] using scanning flow cell (SFC)-ICP-MS measurements during 1000 potential cycles in AST conditions (Figures S18 and S19, Supporting Information). The average thickness of Pt/TiWC was ≈2 ML, indicating that a significant portion of the particles are completely covered with Pt shell. However, the number of dissolved core metals after the potential cycles was smaller in the case of Pt/TaC_0.6 ML by approximately two orders of magnitude, and the difference was even larger (up to around three orders of magnitude) when the dissolution amount observed during the initial stabilization at the open circuit is included. Meanwhile, although the fraction of dissolved Pt shell was slightly smaller for Pt/TaC_0.6 ML, its shell was more vulnerable to dissolution during the potential cycles. This is likely attributable to its low shell coverage, as a core completely covered

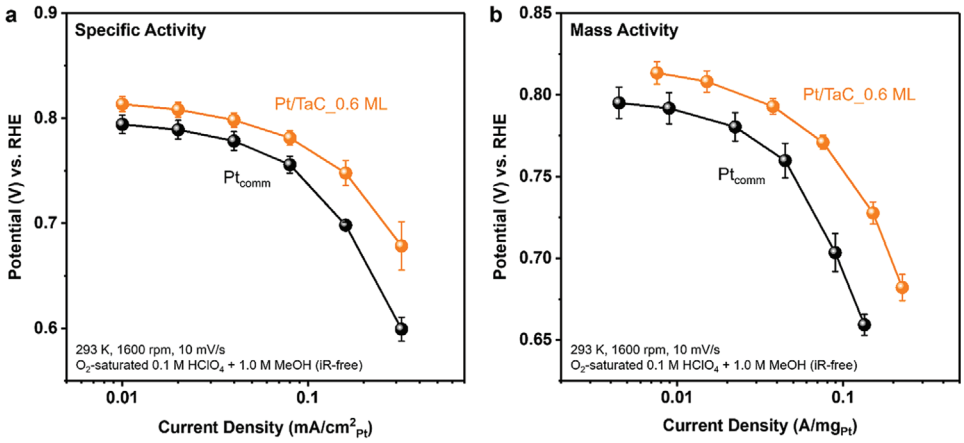

Figure 6. Electrocatalytic oxygen reduction characteristics under the presence of methanol. a) Specific and b) mass ORR activities of Pt_{comm} and Pt/TaC_0.6 ML (obtained from ORR curves shown in Figure S22, Supporting Information) measured in O_2-saturated 0.1 M $HClO_4$ containing 1.0 M MeOH at a scan rate of 10 mV s^{-1} and a rotation speed of 1600 rpm. Calculations of activities were performed after averaging the forward and backward scans, and the error bars show standard deviations obtained from at least three independent measurements.

with the shell is protected from surface oxidation,[8] which weakens chemical adhesion between the core and shell.[7] The highly durable characteristics of Pt/TaC nanoparticles with different dimensions and shell coverages were discussed in a separate study focusing on electrochemical stability.[44]

We studied the development of the electrochemically active surface area (ECSA) of Pt_{comm} and Pt/TaC nanoparticles before and after the AST (Figure 5b; Figure S20, Supporting Information). Based on the adsorption/desorption charges in the H_{upd} region, the ECSA decreased ≈20% for Pt_{comm}, and less than 1% for Pt/TaC_0.6 ML. Interestingly, the CV curves of Pt_{comm} and Pt/TaC_0.6 ML before and after the AST showed a unique difference (Figure S20, Supporting Information). In the case of Pt_{comm}, both currents originating from adsorption and desorption of hydrogen and oxygen species decreased in similar proportions. On the other hand, for Pt/TaC_0.6 ML the current decrease was most apparent within the potential region related to oxygen species. Additionally, the H_{upd} profile changes for Pt/TaC_0.6 ML suggest the possibility of rearrangement or dissolution/redeposition of Pt atoms on the TaC surface during potential cycling.[45–47] As Pt favors forming chemical bonds with metals in TMCs rather than carbon or oxygen in the passivation layer,[7] Pt might rearrange as the surface oxidation of the TaC core occurs. The decrease in ORR performance after the AST was more significant in Pt/TaC than Pt_{comm} (Figure S21, Supporting Information), and this could be attributed to the thickening of TaO_x passivation layer and the rearrangement of Pt atoms, as the ORR activity of Pt is strongly dependent on exposed facets and the coordination environment at the surface.[46,47]

2.4. Oxygen Reduction Characteristics of Pt/TaC Under the Presence of Methanol

Even in the most advanced DMFCs, the diffusion of methanol from the anodic to the cathodic chamber through the membrane is inevitable.[48,49] This methanol crossover causes MOR to take place at the cathode, which results in the negative shift of cathodic potential and CO poisoning that significantly decreases the overall cell voltage.[50,51] Therefore, it is important to develop methanol-resistant ORR catalysts for DMFC cathodes. While state-of-the-art PtRu alloy catalysts can manage methanol crossover and CO poisoning to some extent, the kinetics for the ORR are sluggish under these conditions.[32,52,53]

We investigated the ORR characteristics of Pt/TaC in the presence of methanol in order to evaluate the feasibility of Pt/TaC under more realistic DMFC cathodic conditions. Figure S22 (Supporting Information) shows ORR polarization curves of Pt_{comm} and Pt/TaC_0.6 ML measured in O_2-saturated 0.1 M $HClO_4$ containing 1.0 M methanol. Since MOR and ORR compete for the same catalytic sites, we could not calculate activities by removing the background currents of the Ar-saturated electrolyte. We therefore averaged the forward and backward scans and then calculated specific and mass activities, which are summarized in **Figure 6**a,b, respectively. Pt/TaC showed significantly higher activities compared to those of Pt_{comm}. In particular, the mass activity of Pt/TaC was more than two times that of Pt_{comm} at the potential above 0.7 V (Figure S23, Supporting Information). This difference could be attributed to higher CO oxidation and MOR performances of Pt/TaC. Since the electrolytes used in the electrochemical analysis of both catalysts had identical methanol concentrations and were saturated with O_2, Pt/TaC which can manage methanol faster than Pt_{comm} would be able to reduce a larger number of oxygen molecules per active site. As a result, Pt/TaC manifested a significantly higher ORR activity than Pt_{comm} in the presence of methanol, and the feasibility of Pt/TaC catalysts for both electrodes of DMFC could be clearly verified.

3. Conclusion

In this study, Pt/TaC core–shell nanoparticles were synthesized and applied as electrocatalysts for the MOR and ORR. TaC was chosen as a core material due to its high stability at low pH values and high potential. The presence of Pt during the carburization process enabled the synthesis of Pt/TaC nanoparticles at a milder temperature, presumably via unique catalytic interactions

of Pt with H_2 and CH_4. Pt/TaC with sub-monolayer shell thicknesses showed superior MOR activity compared to that of Pt_{comm} as a result of weaker CO binding strength on Pt and the participation of surface-oxidized TaC in the reaction. In the presence of methanol, Pt/TaC manifested a significantly higher ORR activity compared to Pt_{comm}. Stability of Pt/TaC during electrochemical cycling was also thoroughly investigated based on a variety of analytical techniques, which unveiled that the portion of dissolved core material during 10 800 cycles of AST was around three orders of magnitude smaller than that of the previously reported Pt/TiWC system. This work shows that Pt/TaC could serve as an early stage platform for designing stable core–shell nanoparticles for applications in diverse electrochemical and catalytic systems, given their high versatility and wide room for further enhancements by compositional and structural engineering. Furthermore, our study opens up opportunities to tailor the property of core–shell nanoparticles by demonstrating that core materials that are sufficiently stable can take part in catalysis and modify reaction kinetics.

4. Experimental Section

Experimental methods including the detailed procedures for the synthesis, physical characterization, and electrochemical analysis are provided in the Supporting Information.

Supporting Information

Supporting Information is available from the Wiley Online Library or from the author.

Acknowledgements

Z.W., J.S.K., Y.S.-H., and Y.R.-L. acknowledge that this work was supported by Eni S.p.A. M.L. and D.G. acknowledges the Federal Ministry of Education and Research (BMBF) in the framework of NanoMatFutur (SynKat) for financial support (project number 03XP0265). This research used beamline 8-ID (ISS) of the National Synchrotron Light Source II, and the Center for Functional Nanomaterials, U.S. Department of Energy (DOE) Office of Science User Facilities operated for the DOE Office of Science by Brookhaven National Laboratory under contract No. DE-SC0012704 (Proposal GU-304417 and DT-306032).

Conflict of Interest

The authors declare no conflict of interest.

Author Contributions

Z.W. and J.S.K. contributed equally to this work. Z.W., J.S.K., Y.S.-H., M.L., and Y.R.-L. conceived this study. Z.W. synthesized the materials and conducted physical characterizations. J.S.K. designed and conducted an electrochemical analysis. D.G. and P.P. carried out the stability-related in situ analysis. D.S.G. and D.Z. performed a quantitative analysis of the EXAFS spectra. H.-K.L. performed the theoretical calculations. The manuscript was written by J.S.K., Z.W., Y.R.-L., M.L., and Y.S.-H. All authors discussed the manuscript and the results.

Data Availability Statement

The data that support the findings of this study are available from the corresponding author upon reasonable request.

Keywords

core–shell nanoparticles, electrocatalysis, fuel cells, methanol oxidation, oxygen reduction, tantalum carbide

Received: November 29, 2023
Revised: February 13, 2024
Published online:

[1] B. C. H. Steele, A. Heinzel, *Nature* **2001**, *414*, 345.
[2] J. N. Tiwari, R. N. Tiwari, G. Singh, K. S. Kim, *Nano Energy* **2013**, *2*, 553.
[3] Z. Xia, X. Zhang, H. Sun, S. Wang, G. Sun, *Nano Energy* **2019**, *65*, 104048.
[4] X. Zhao, M. Yin, L. Ma, L. Liang, C. Liu, J. Liao, T. Lu, W. Xing, *Energy Environ. Sci.* **2011**, *4*, 2736.
[5] N. Kakati, J. Maiti, S. H. Lee, S. H. Jee, B. Viswanathan, Y. S. Yoon, *Chem. Rev.* **2014**, *114*, 12397.
[6] Y. Tong, X. Yan, J. Liang, S. X. Dou, *Small* **2020**, *16*, 1904126.
[7] S. T. Hunt, M. Milina, A. C. Alba-Rubio, C. H. Hendon, J. A. Dumesic, Y. Román-Leshkov, *Science* **2016**, *352*, 974.
[8] D. Göhl, A. Garg, P. Paciok, K. J. J. Mayrhofer, M. Heggen, Y. Shao-Horn, R. E. Dunin-Borkowski, Y. Román-Leshkov, M. Ledendecker, *Nat. Mater.* **2020**, *19*, 287.
[9] M. C. Weidman, D. V. Esposito, Y.-C. Hsu, J. G. Chen, *J. Power Sources* **2012**, *202*, 11.
[10] Y. C. Kimmel, X. Xu, W. Yu, X. Yang, J. G. Chen, *ACS Catal.* **2014**, *4*, 1558.
[11] D. Göhl, H. Rue*β*, M. Pander, A. R. Zeradjanin, K. J. J. Mayrhofer, J. M. Schneider, A. Erbe, M. Ledendecker, *J. Electrochem. Soc.* **2020**, *167*, 021501.
[12] D. Göhl, H. Rue*β*, S. Schlicht, A. Vogel, M. Rohwerder, K. J. J. Mayrhofer, J. Bachmann, Y. Román-Leshkov, J. M. Schneider, M. Ledendecker, *ChemElectroChem* **2020**, *7*, 2404.
[13] V. G. Sevast'yanov, E. P. Simonenko, N. A. Ignatov, Y. S. Ezhov, N. T. Kuznetsov, *Inorg. Mater.* **2010**, *46*, 495.
[14] N. S. Alhajri, H. Yoshida, D. H. Anjum, A. T. Garcia-Esparza, J. Kubota, K. Domen, K. Takanabe, *J. Mater. Chem. A.* **2013**, *1*, 12606.
[15] W. C. Connor, J. L. Falconer, *Chem. Rev.* **1995**, *95*, 759.
[16] V. V. Lesnyak, V. K. Yatsimirskii, O. Y. Boldyreva, T. D. Kinder, *Theor. Exp. Chem.* **2008**, *44*, 189.
[17] E. P. J. Mallens, J. H. B. J. Hoebink, G. B. Marin, *Catal. Lett.* **1995**, *33*, 291.
[18] P. A. Bui, D. G. Vlachos, P. R. Westmoreland, *Surf. Sci.* **1997**, *385*, L1029.
[19] D. E. Ramaker, B. L. Mojet, M. T. G. Oostenbrink, J. T. Miller, D. C. Koningsberger, *Phys. Chem. Chem. Phys.* **1999**, *1*, 2293.
[20] Y. Lei, J. Jelic, L. C. Nitsche, R. Meyer, J. Miller, *Top. Catal.* **2011**, *54*, 334.
[21] Z. Wang, A. Garg, L. Wang, H. He, A. Dasgupta, D. Zanchet, M. J. Janik, R. M. Rioux, Y. Román-Leshkov, *ACS Catal.* **2020**, *10*, 6763.
[22] A. Garg, D. S. Gonçalves, Y. Liu, Z. Wang, L. Wang, J. S. Yoo, A. Kolpak, R. M. Rioux, D. Zanchet, Y. Román-Leshkov, *ACS Catal.* **2019**, *9*, 7090.
[23] G. N. Derry, Z. Ji-Zhong, *Phys. Rev. B* **1989**, *39*, 1940.
[24] H. Zhu, R. Ramprasad, *J. Appl. Phys.* **2011**, *109*, 083719.
[25] H. Yan, C. Tian, L. Wang, A. Wu, M. Meng, L. Zhao, H. Fu, *Angew. Chem., Int. Ed.* **2015**, *54*, 6325.
[26] B. Hammer, J. K. Nørskov, *Nature* **1995**, *376*, 238.
[27] B. Hammer, J. K. Nørskov, *Adv. Catal.* **2000**, *45*, 71.
[28] P. Strasser, S. Koh, T. Anniyev, J. Greeley, K. More, C. Yu, Z. Liu, S. Kaya, D. Nordlund, H. Ogasawara, M. F. Toney, A. Nilsson, *Nat. Chem.* **2010**, *2*, 454.

[29] S. Kattel, G. Wang, *J. Chem. Phys.* **2014**, *141*, 124713.
[30] C. Lamy, J.-M. Léger, J. Clavilier, R. Parsons, *J. Electroanal. Chem.* **1983**, *150*, 71.
[31] P. Urchaga, S. Baranton, C. Coutanceau, G. Jerkiewicz, *Langmuir* **2012**, *28*, 13094.
[32] M. J. Lee, J. S. Kang, Y. S. Kang, D. Y. Chung, H. Shin, C.-Y. Ahn, S. Park, M.-J. Kim, S. Kim, K.-S. Lee, Y.-E. Sung, *ACS Catal.* **2016**, *6*, 2398.
[33] H. A. Gasteiger, N. M. Markovic, P. N. Ross Jr., *J. Phys. Chem.* **1995**, *99*, 8290.
[34] D. Y. Chung, K.-J. Lee, Y.-E. Sung, *J. Phys. Chem. C* **2016**, *120*, 9028.
[35] N. P. Lebedeva, M. T. M. Koper, J. M. Feliu, R. A. van Santen, *J. Phys. Chem. B* **2002**, *106*, 12938.
[36] H. Wang, H. Abruña, *J. Phys. Chem. Lett.* **2015**, *6*, 1899.
[37] S. W. Lee, S. Chen, W. Sheng, N. Yabuuchi, Y.-T. Kim, T. Mitani, E. Vescovo, Y. Shao-Horn, *J. Am. Chem. Soc.* **2009**, *131*, 15669.
[38] P. Urchaga, S. Baranton, C. Coutanceau, G. Jerkiewicz, *Langmuir* **2012**, *28*, 3658.
[39] U. A. Paulus, T. J. Schmidt, H. A. Gasteiger, R. J. Behm, *J. Electroanal. Chem.* **2001**, *495*, 134.
[40] J. K. Nørskov, J. Rossmeisl, A. Logadottir, L. Lindqvist, J. R. Kitchin, T. Bligaard, H. Jónsson, *J. Phys. Chem. B* **2004**, *108*, 17886.
[41] I. E. L. Stephens, A. S. Bondarenko, U. Grønbjerg, J. Rossmeisl, I. Chorkendorff, *Energy Environ. Sci.* **2012**, *5*, 6744.
[42] C. Koenigsmann, W.-p. Zhou, R. R. Adzic, E. Sutter, S. S. Wong, *Nano Lett.* **2010**, *10*, 2806.
[43] R. Wang, D. C. Higgins, M. A. Hoque, D. U. Lee, F. Hassan, Z. Chen, *Sci. Rep.* **2013**, *3*, 2431.
[44] D. Göhl, P. Paciok, Z. Wang, J. S. Kang, M. Heggen, K. J. J. Mayrhofer, Y. Román-Leshkov, M. Ledendecker, *Nano Select* **2023**, *4*, 271.
[45] N. M. Marković, R. R. Adžić, B. D. Cahan, E. B. Yeager, *J. Electroanal. Chem.* **1994**, *377*, 249.
[46] P. P. Lopes, D. Strmcnik, D. Tripkovic, J. G. Connell, V. Stamenkovic, N. M. Markovic, *ACS Catal.* **2016**, *6*, 2536.
[47] D. J. S. Sandbeck, O. Brummel, K. J. J. Mayrhofer, J. Libuda, I. Katsounaros, S. Cherevko, *ChemPhysChem* **2019**, *20*, 2997.
[48] A. Heinzel, V. M. Barragán, *J. Power Sources* **1999**, *84*, 70.
[49] M. Ahmed, I. Dincer, *Int. J. Energy Res.* **2011**, *35*, 1213.
[50] Z. Qi, A. Kaufman, *J. Power Sources* **2002**, *110*, 177.
[51] S. Jang, S. Kim, S. M. Kim, J. Choi, J. Yeon, K. Bang, C.-Y. Ahn, W. Hwang, M. Her, Y.-H. Cho, Y.-E. Sung, M. Choi, *Nano Energy* **2018**, *43*, 149.
[52] J. Zhang, M. B. Vukmirovic, Y. Xu, M. Mavrikakis, R. R. Adzic, *Angew. Chem., Int. Ed.* **2005**, *44*, 2132.
[53] J. Greeley, I. E. L. Stephens, A. S. Bondarenko, T. P. Johansson, H. A. Hansen, T. F. Jaramillo, J. Rossmeisl, I. Chorkendorff, J. K. Nørskov, *Nat. Chem.* **2009**, *1*, 552.